Supporting Information for

Mid-Tropospheric Layer Temperature Record Derived from Satellite Microwave Sounder Observations with Backward Merging Approach

Cheng-Zhi Zou[1*], Hui Xu[2], Xianjun Hao[3], and Qian Liu[3]

[1]Center for Satellite Applications and Research, NOAA/NESDIS, College Park, MD 20740, USA

[2]ESSIC/CISESS, University of Maryland, College Park, MD 20740, USA

[3]Environmental Science and Technology Center, College of Science, George Mason University, Fairfax, VA 22030, USA

*Corresponding author email: Cheng-Zhi.Zou@noaa.gov

Contents of this file

Figures

Figure S1. Monthly mean diurnal anomalies for MSU channel 2 and AMSU-A channel 5 obtained from the semi-physical model and their comparisons to the CCM3 climate model simulations at selected regions.

Figure S2. Inter-satellite differences ($\Delta TB_{jk}=TB_j - TB_k$, colored solid lines) and diurnal anomaly differences ($\Delta D_{jk} = D_j-D_k$, dashed lines) derived from the semi-physical model for (a) over the tropical ocean (20^0S-20^0N), and (b) over the tropical land. Differences were grouped into ascending and descending data separately by adding constant offsets to different satellite pairs for an adjustment. As such, the vertical temperature coordinate does not necessarily represent the actual values or signs of the mean diurnal anomaly differences, but they represent the magnitudes of the seasonal cycle and drifting range of the diurnal anomaly differences. The NOAA-15 diurnal anomalies during the 3.5-year period from 11/1998 to 07/2002 were predicted from the physical model based on regression coefficients obtained from its overlaps with RTMT during 08/2002-12/2017.

Figure S3. Same as Figure S2 except for the Southern midlatitudes (20^0S-60^0S).

Figure S4. Same as Figure S2 except for the Northern midlatitudes (20^0N-60^0N).

Figure S5. Same as Figure S2 except for the Southern polar region (60^0S-82.5^0S).

Figure S6. Same as Figure S2 except for the Northern polar region (60^0N-82.5^0N).

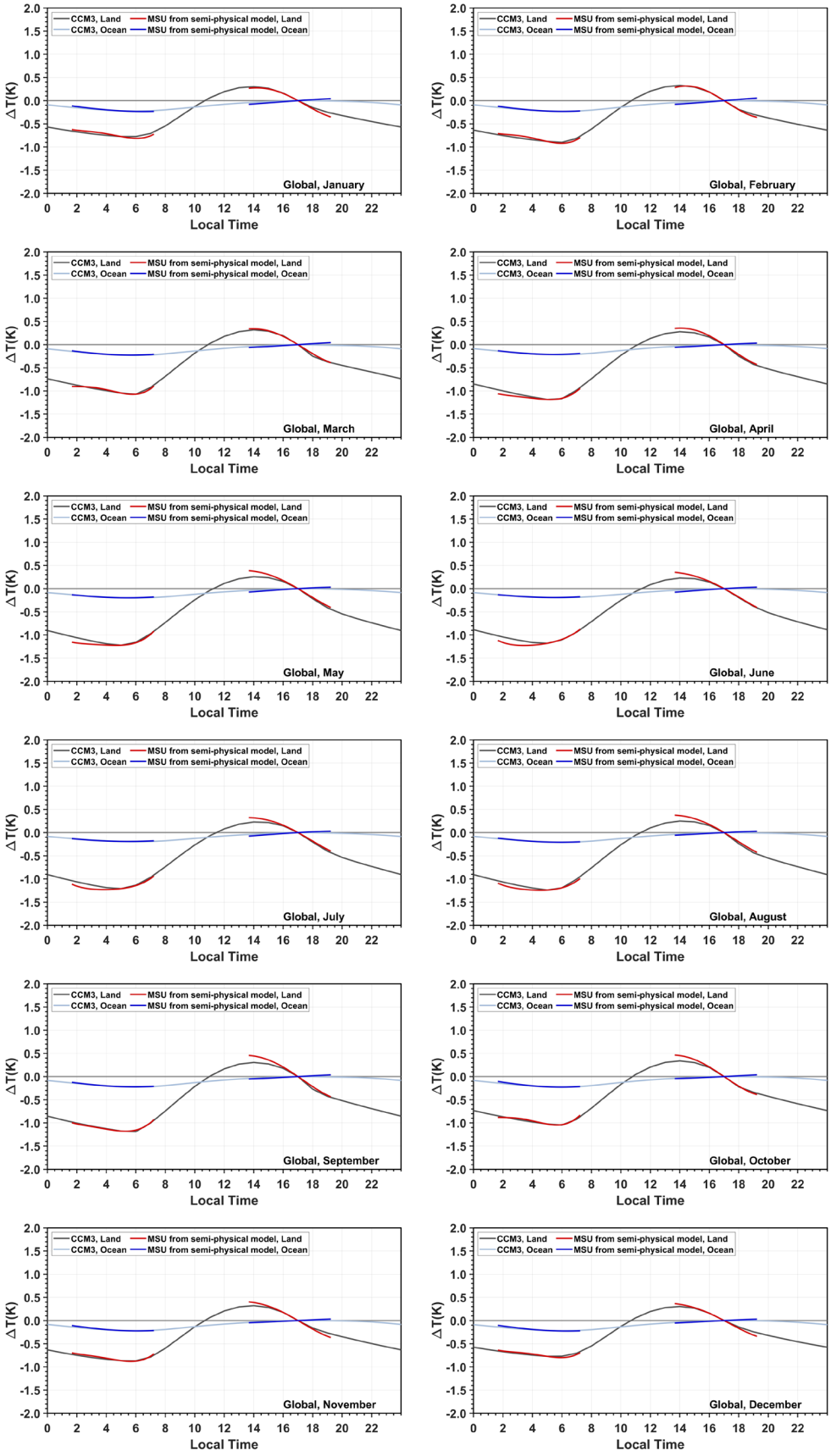
CCM3, Land
MSU from semi-physical model, Land
CCM3, Ocean
MSU from semi-physical model, Ocean
ΔT(K)
Local Time
Global, January
Global, February
Global, March
Global, April
Global, May
Global, June
Global, July
Global, August
Global, September
Global, October
Global, November
Global, December

Figure S1A

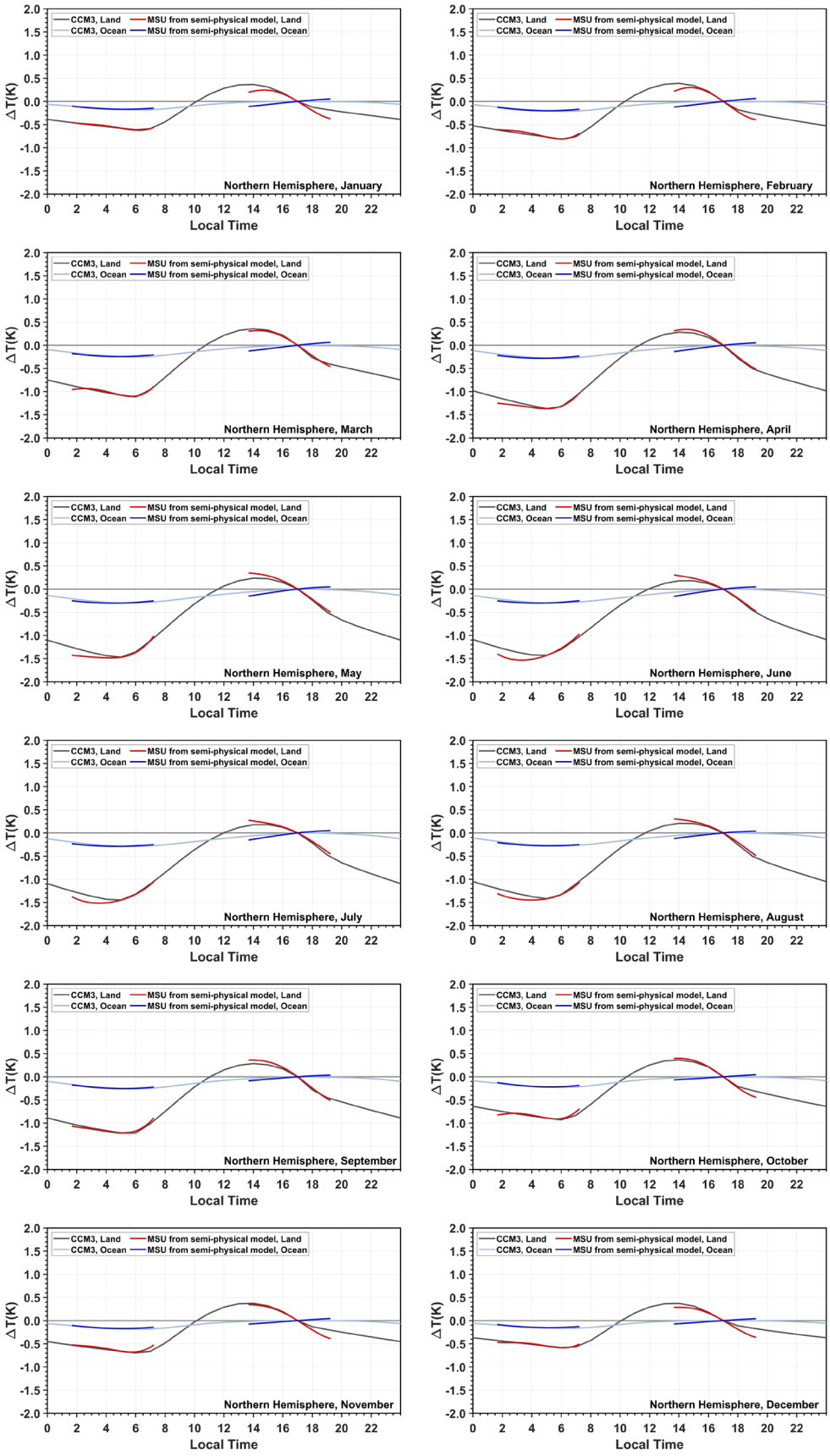
CCM3, Land
MSU from semi-physical model, Land
CCM3, Ocean
MSU from semi-physical model, Ocean
ΔT(K)
Local Time
Northern Hemisphere, January
Northern Hemisphere, February
Northern Hemisphere, March
Northern Hemisphere, April
Northern Hemisphere, May
Northern Hemisphere, June
Northern Hemisphere, July
Northern Hemisphere, August
Northern Hemisphere, September
Northern Hemisphere, October
Northern Hemisphere, November
Northern Hemisphere, December

Figure S1B

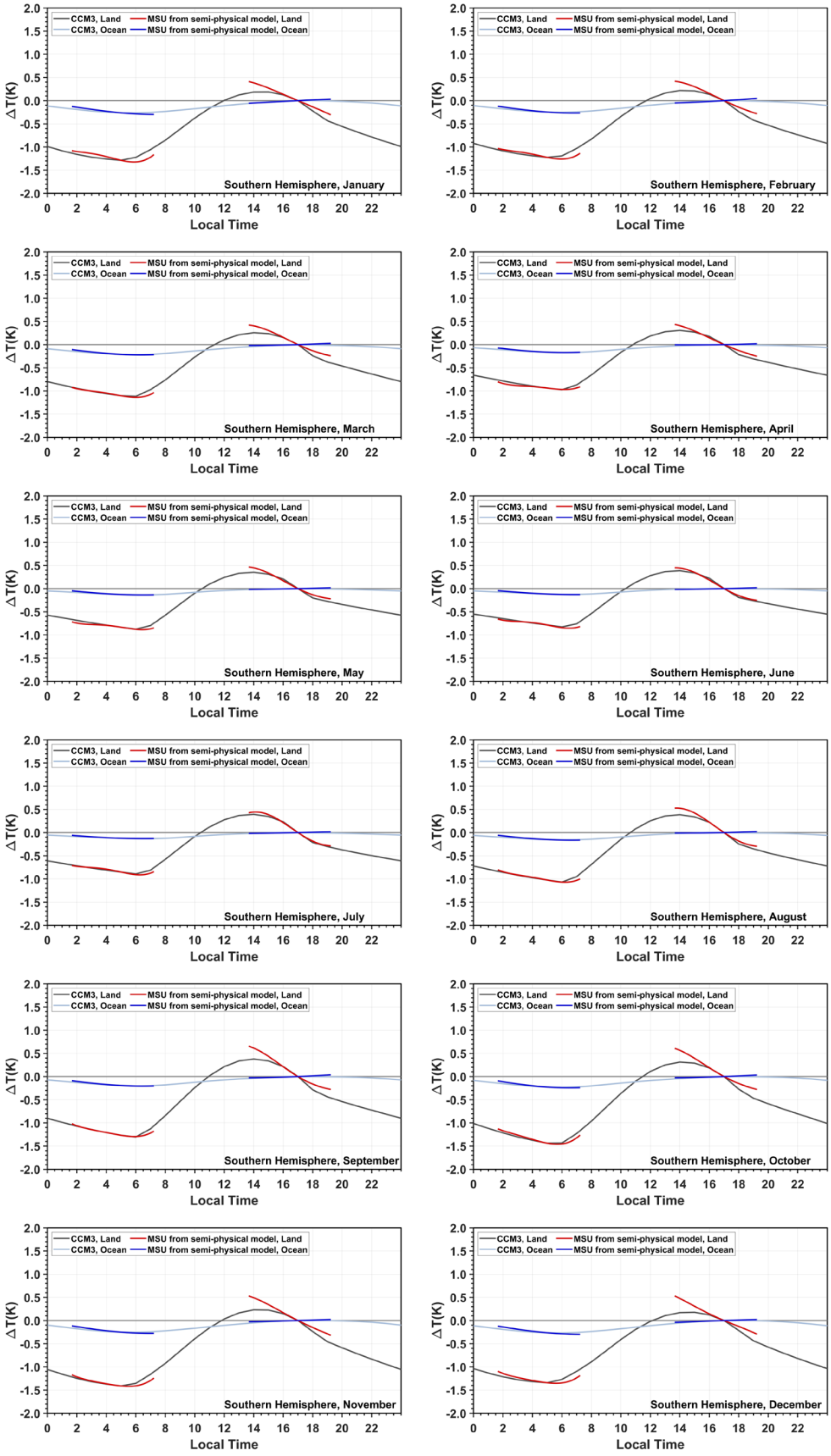
CCM3, Land
MSU from semi-physical model, Land
CCM3, Ocean
MSU from semi-physical model, Ocean
ΔT(K)
Local Time
Southern Hemisphere, January
Southern Hemisphere, February
Southern Hemisphere, March
Southern Hemisphere, April
Southern Hemisphere, May
Southern Hemisphere, June
Southern Hemisphere, July
Southern Hemisphere, August
Southern Hemisphere, September
Southern Hemisphere, October
Southern Hemisphere, November
Southern Hemisphere, December

Figure S1C

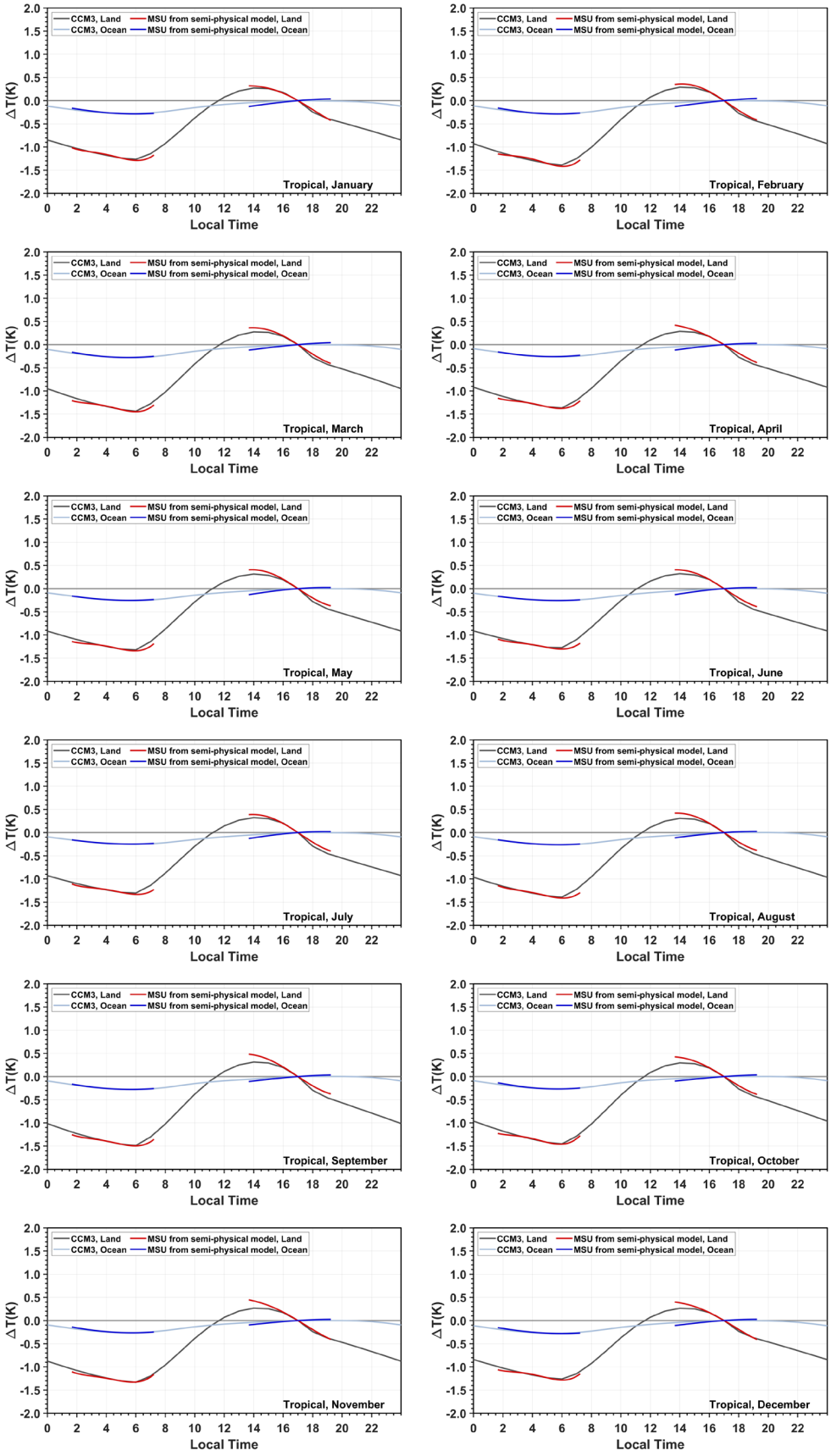
CCM3, Land
MSU from semi-physical model, Land
CCM3, Ocean
MSU from semi-physical model, Ocean
ΔT(K)
Local Time
Tropical, January
Tropical, February
Tropical, March
Tropical, April
Tropical, May
Tropical, June
Tropical, July
Tropical, August
Tropical, September
Tropical, October
Tropical, November
Tropical, December

Figure S1D

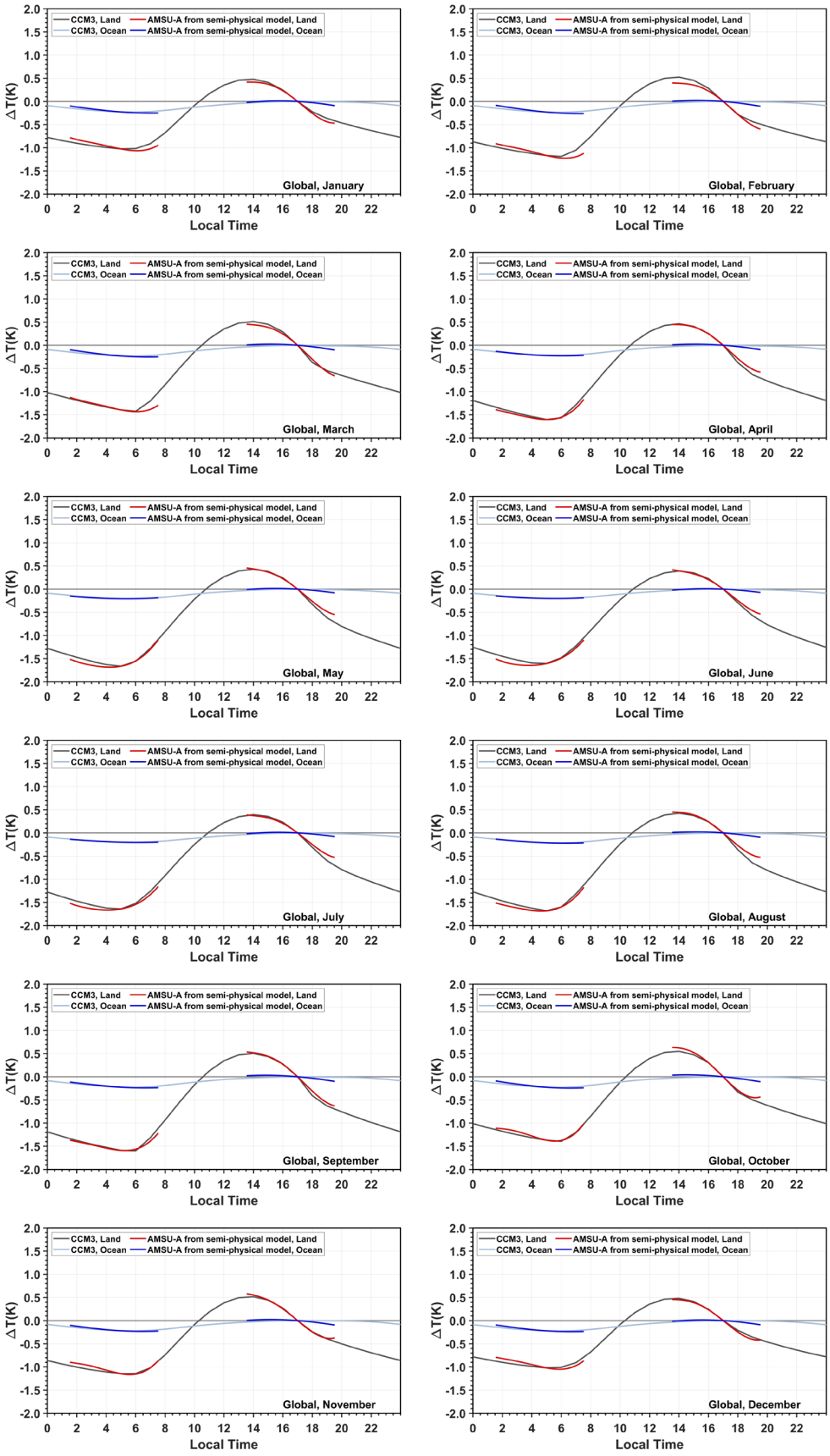
CCM3, Land
CCM3, Ocean
AMSU-A from semi-physical model, Land
AMSU-A from semi-physical model, Ocean
ΔT(K)
Local Time
Global, January
Global, February
Global, March
Global, April
Global, May
Global, June
Global, July
Global, August
Global, September
Global, October
Global, November
Global, December

Figure S1E

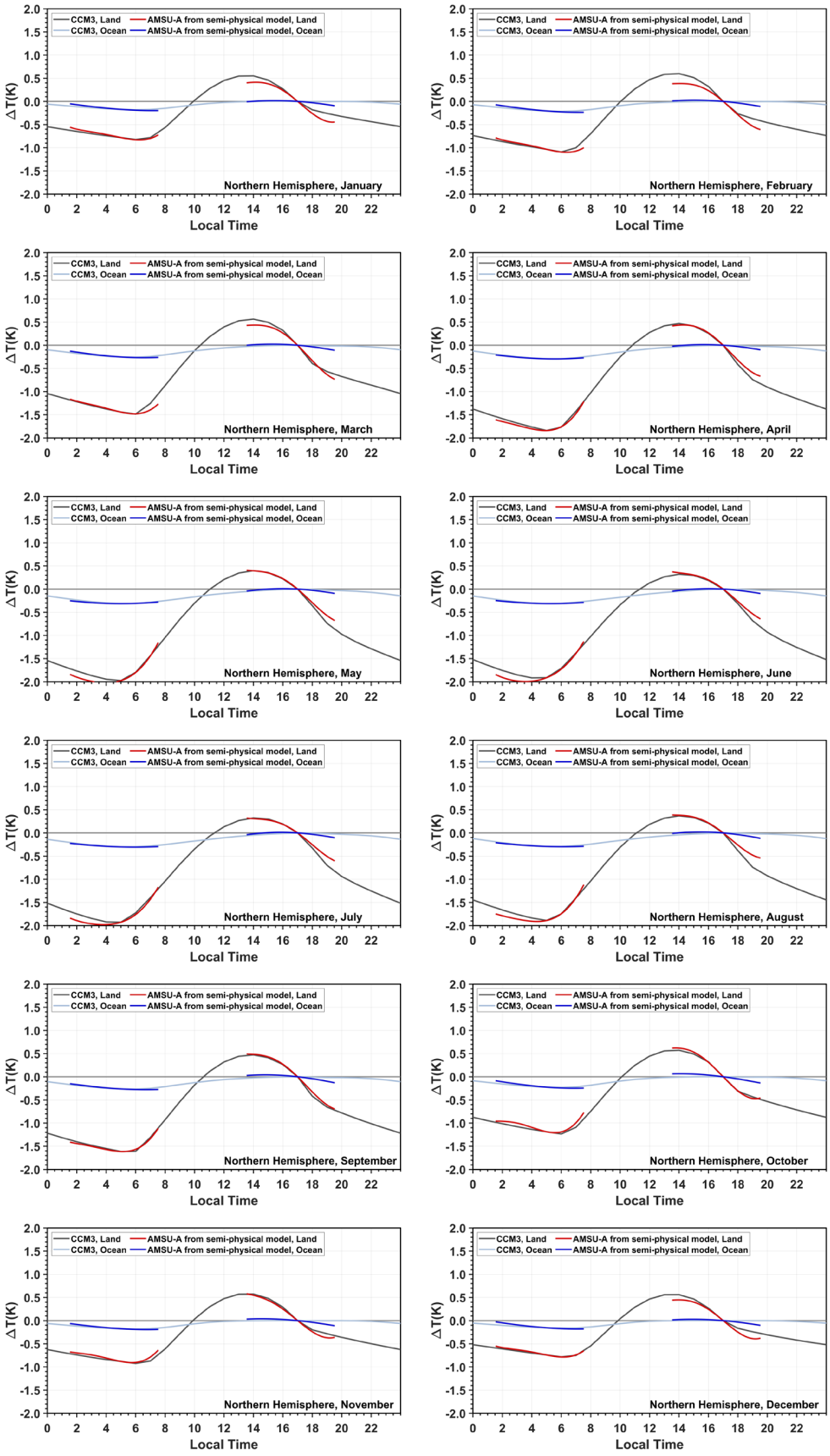
CCM3, Land
CCM3, Ocean
AMSU-A from semi-physical model, Land
AMSU-A from semi-physical model, Ocean
ΔT(K)
Local Time
Northern Hemisphere, January
Northern Hemisphere, February
Northern Hemisphere, March
Northern Hemisphere, April
Northern Hemisphere, May
Northern Hemisphere, June
Northern Hemisphere, July
Northern Hemisphere, August
Northern Hemisphere, September
Northern Hemisphere, October
Northern Hemisphere, November
Northern Hemisphere, December

Figure S1F

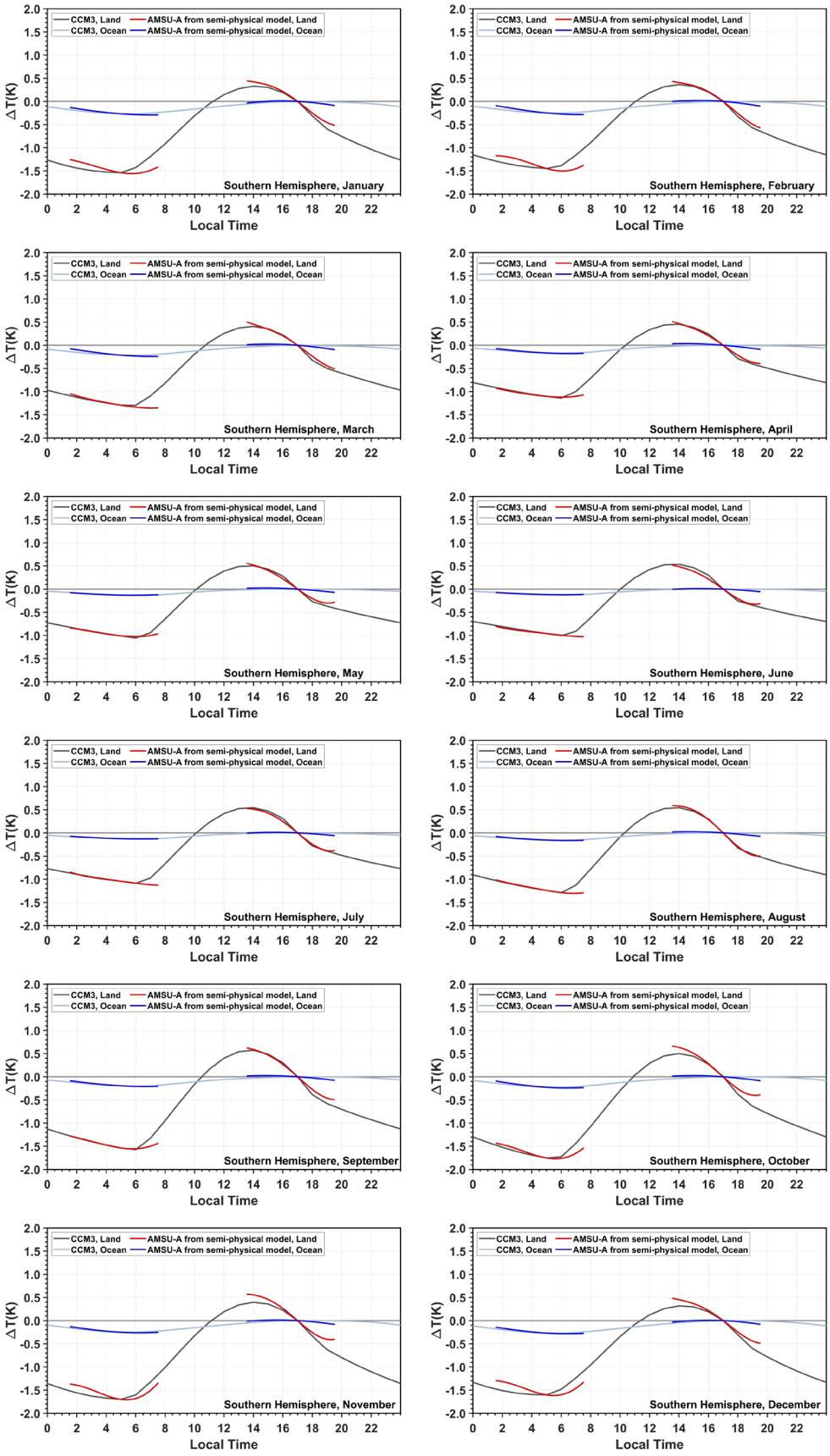
CCM3, Land
CCM3, Ocean
AMSU-A from semi-physical model, Land
AMSU-A from semi-physical model, Ocean
ΔT(K)
Local Time
Southern Hemisphere, January
Southern Hemisphere, February
Southern Hemisphere, March
Southern Hemisphere, April
Southern Hemisphere, May
Southern Hemisphere, June
Southern Hemisphere, July
Southern Hemisphere, August
Southern Hemisphere, September
Southern Hemisphere, October
Southern Hemisphere, November
Southern Hemisphere, December

Figure S1G

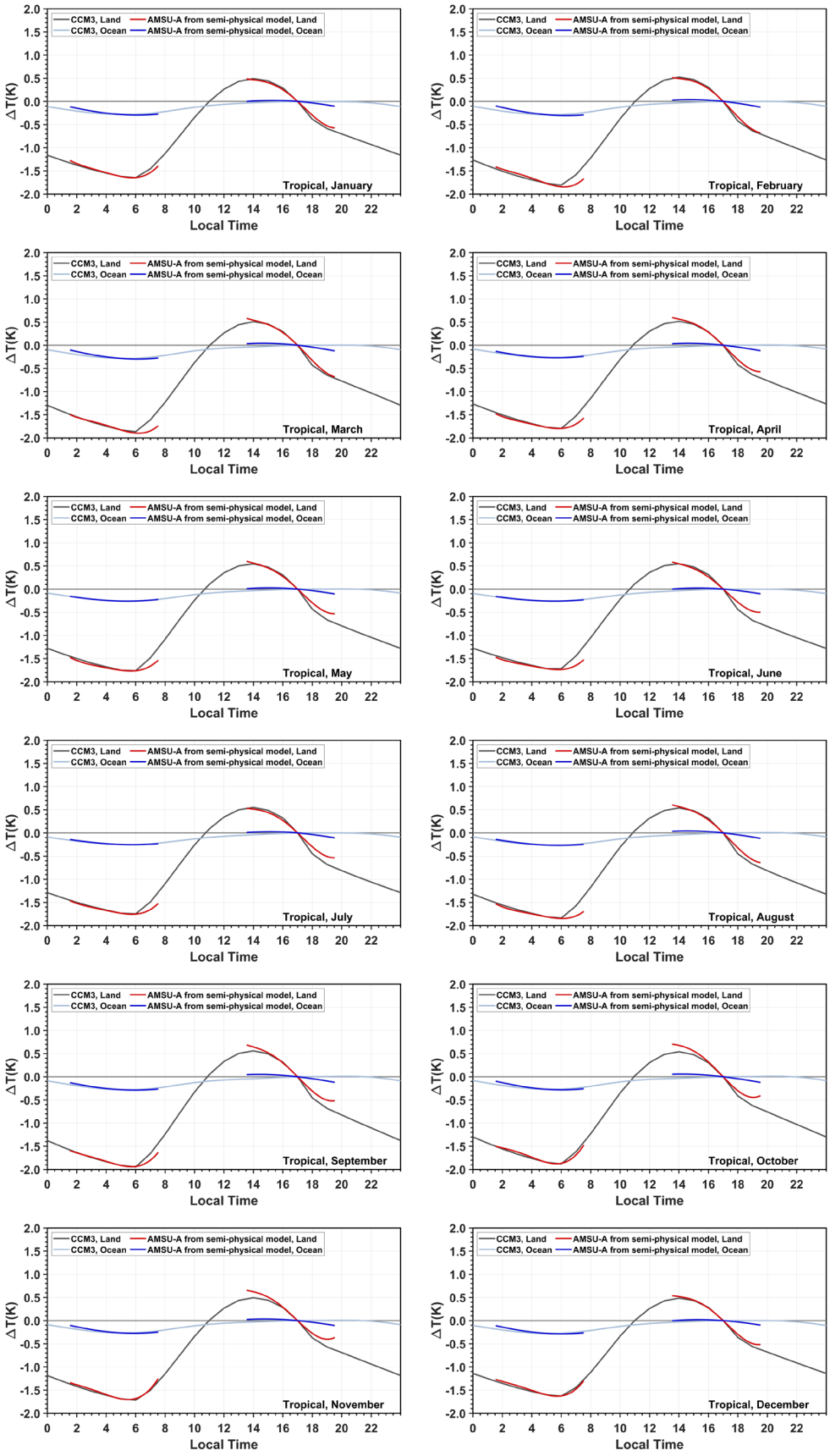
CCM3, Land
CCM3, Ocean
AMSU-A from semi-physical model, Land
AMSU-A from semi-physical model, Ocean
ΔT(K)
Local Time
Tropical, January
Tropical, February
Tropical, March
Tropical, April
Tropical, May
Tropical, June
Tropical, July
Tropical, August
Tropical, September
Tropical, October
Tropical, November
Tropical, December

Figure S1H

Figure S1. Monthly mean diurnal anomalies for MSU channel 2 and AMSU-A channel 5 obtained from the semi-physical model and their comparisons to the CCM3 climate model simulations at selected regions. (a) MSU over the global land and ocean; (b) MSU over the Northern Hemispheric land and ocean; (c) MSU over the Southern Hemispheric land and ocean; (d) MSU over the topical (20^0S-20^0N) land and ocean; (e) AMSU-A over the global land and ocean; (f) AMSU-A over the Northern Hemispheric land and ocean; (g) AMSU-A over the Southern Hemispheric land and ocean; (h) AMSU-A over the topical (20^0S-20^0N) land and ocean. The left and right branches in the semi-physical model solutions are for descending and ascending orbits, respectively. The semi-physical model included both the diurnal and semi-diurnal components over land but only the diurnal component over ocean for the MSU and AMSU-A satellites. The reference points in the semi-physical model solutions are the means of the LECTs, which are 17:00 pm (5:00 am) for the ascending (descending) orbit for both the MSU and AMSU-A satellites. The reference points in the semi-physical model solutions are forced to match the CCM3 simulations at the same times to aid in comparisons between the two types of the diurnal anomalies.

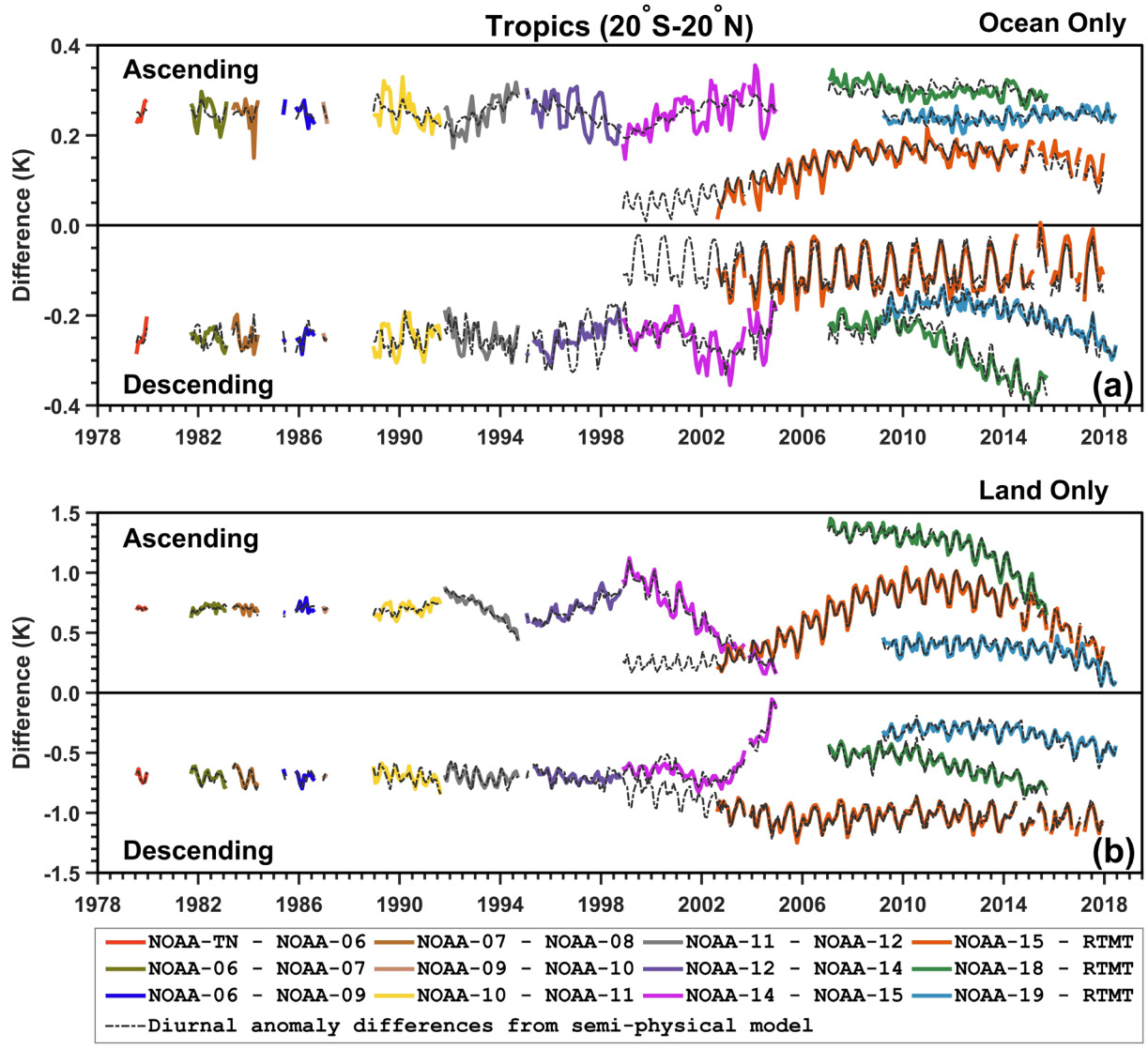

Figure S2. Inter-satellite differences ($\Delta TB_{jk}=TB_j - TB_k$, colored solid lines) and diurnal anomaly differences ($\Delta D_{jk} = D_j-D_k$, dashed lines) derived from the semi-physical model for (a) over the tropical ocean (20^0S-20^0N), and (b) over the tropical land. Differences were grouped into ascending and descending data separately by adding constant offsets to different satellite pairs for an adjustment. As such, the vertical temperature coordinate does not necessarily represent the actual values or signs of the mean diurnal anomaly differences, but they represent the magnitudes of the seasonal cycle and drifting range of the diurnal anomaly differences. The NOAA-15 diurnal anomalies during the 3.5-year period from 11/1998 to 07/2002 were predicted from the physical model based on regression coefficients obtained from its overlaps with RTMT during 08/2002-12/2017.

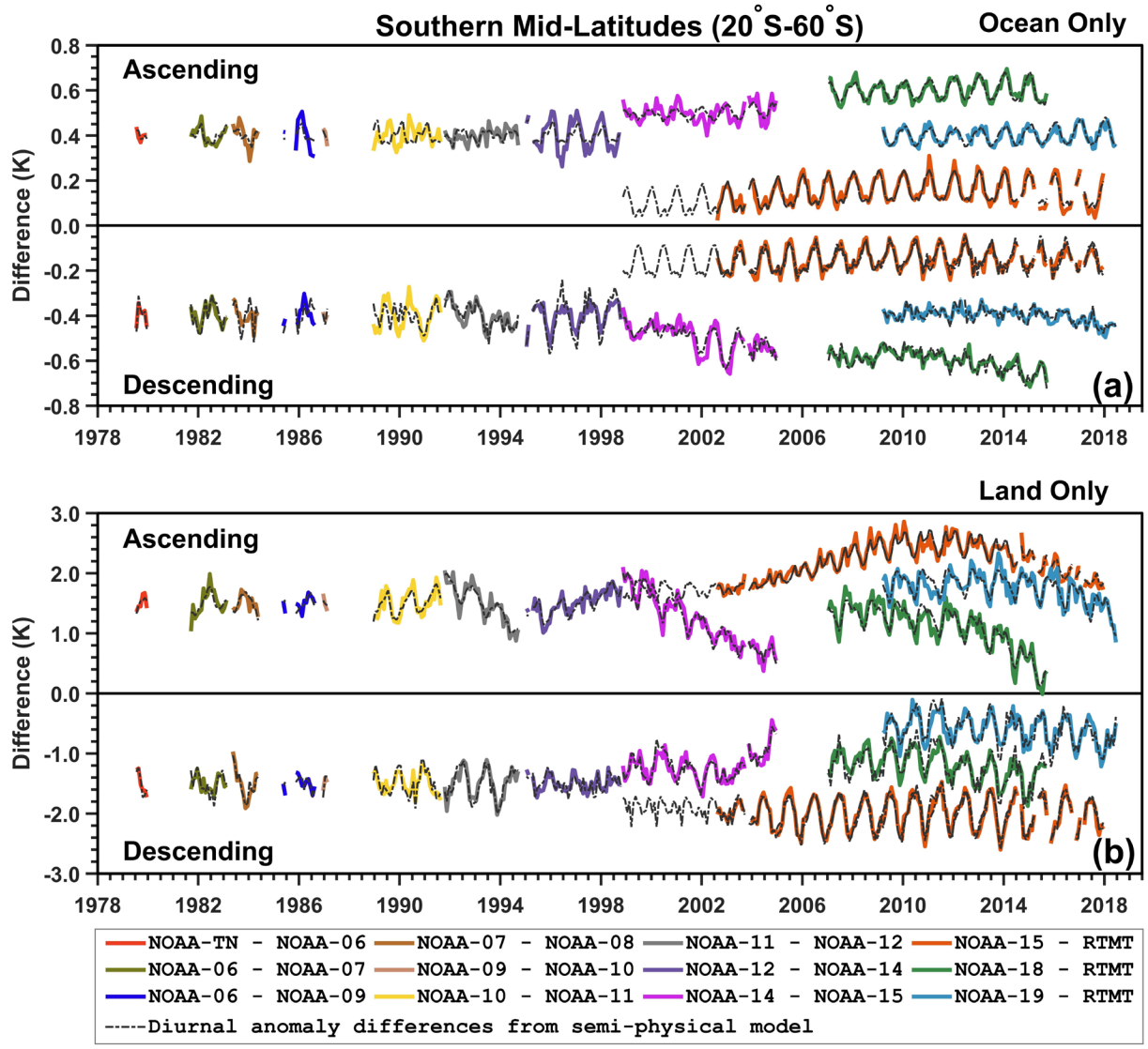

Figure S3. Same as Figure S2 except for the Southern midlatitudes (20^0S-60^0S).

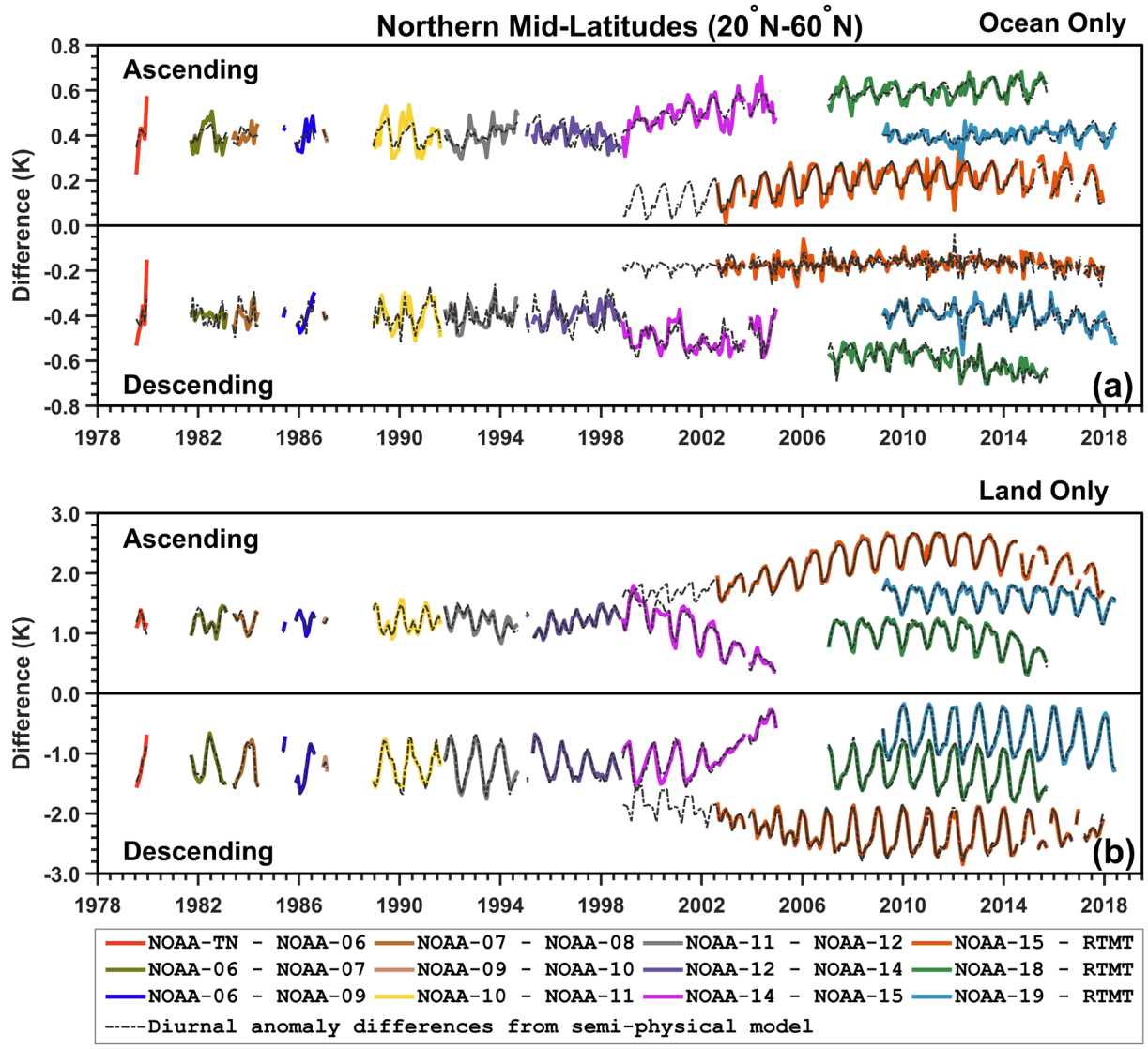

Figure S4. Same as Figure S2 except for the Northern midlatitudes (20^0N-60^0N).

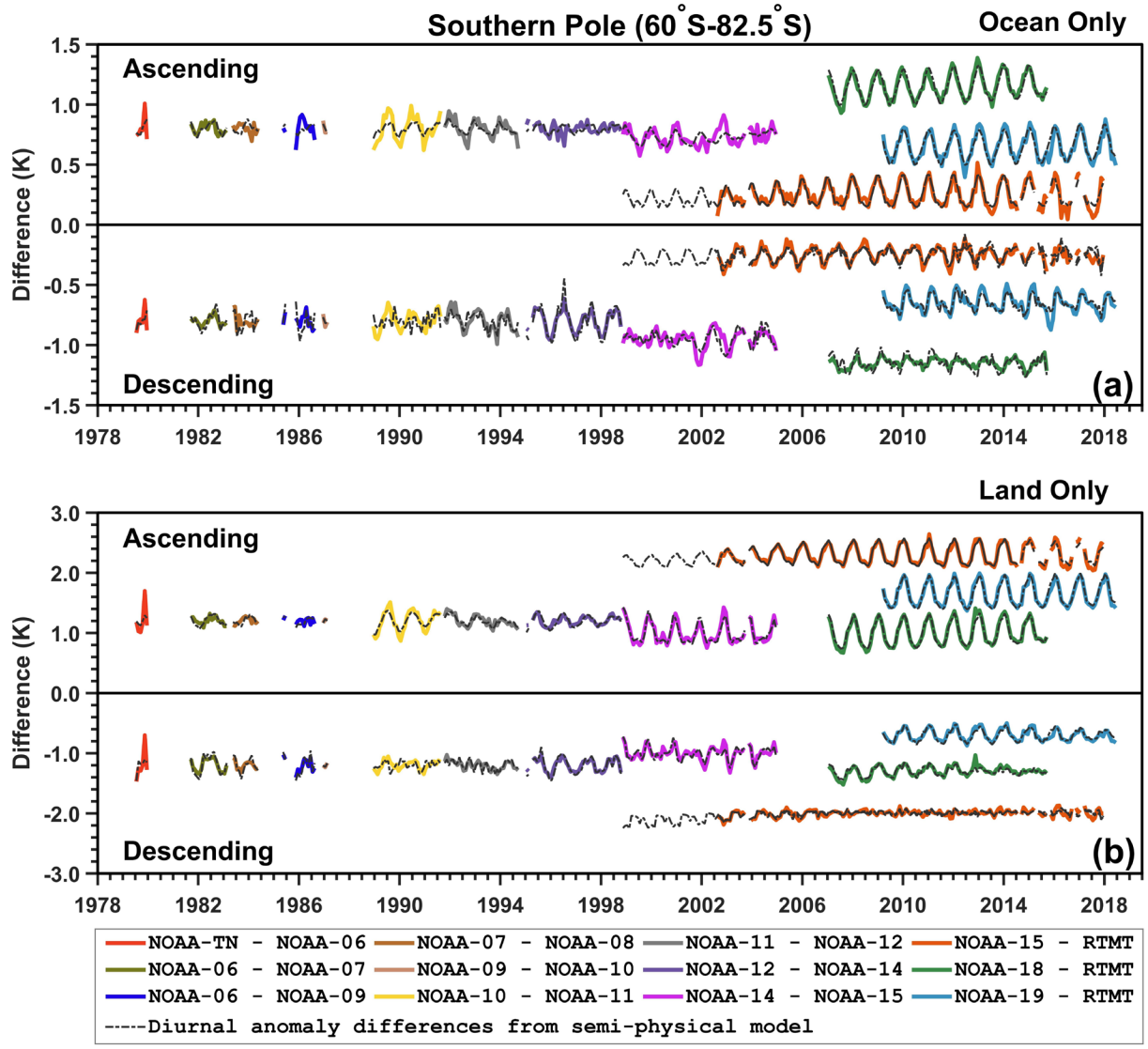

Figure S5. Same as Figure S2 except for the Southern polar region (60^0S-82.5^0S).

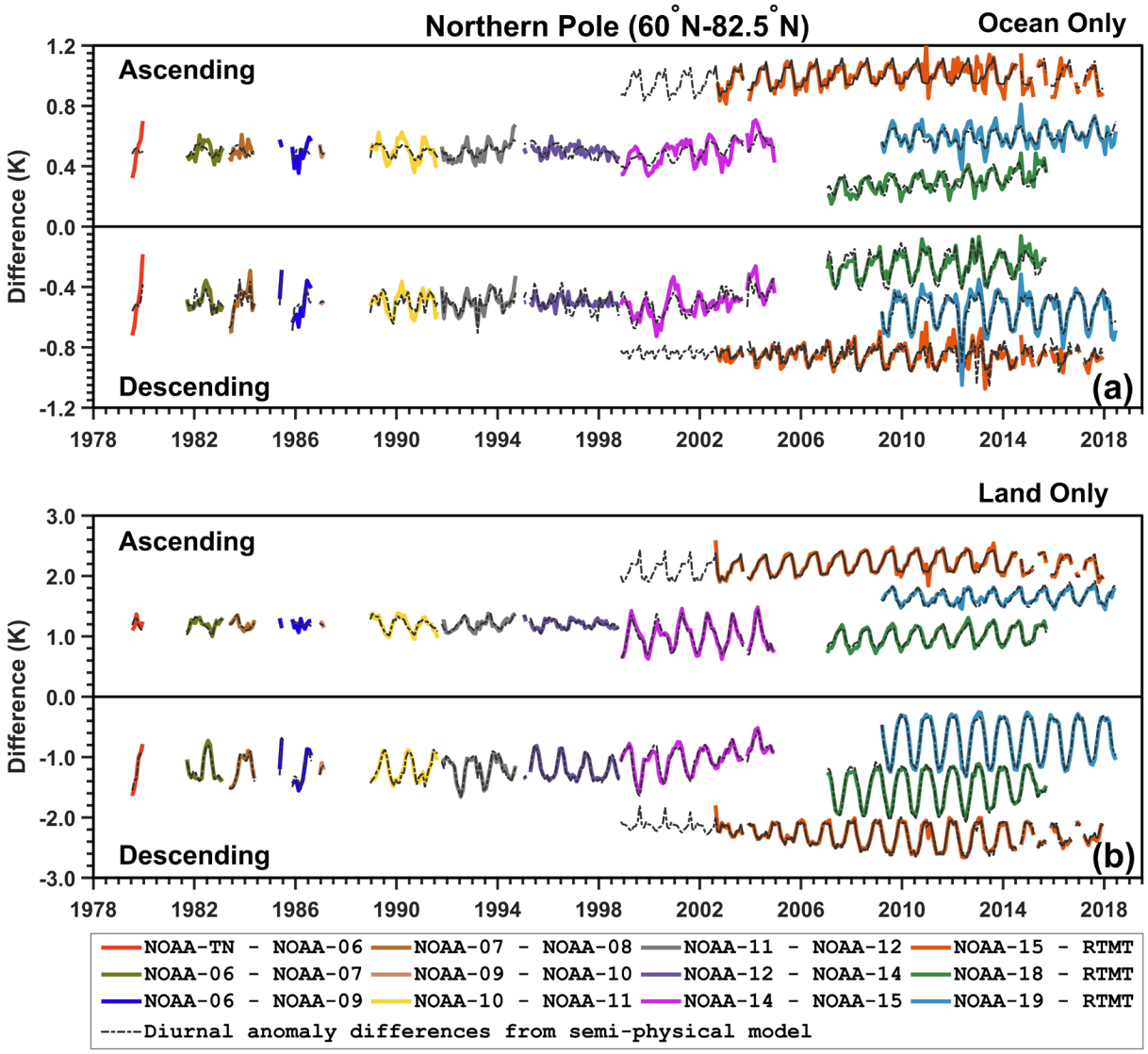

Figure S6. Same as Figure S2 except for the Northern polar region (60^0N-82.5^0N).